Science Bulletin 65 (2020) 1635–1642

Contents lists available at ScienceDirect

Science Bulletin

journal homepage: www.elsevier.com/locate/scib

Article

Chloroplast-like porous bismuth-based core–shell structure for high energy efficiency CO_2 electroreduction

Yi-Rong Wang [1], Ru-Xin Yang [1], Yifa Chen *, Guang-Kuo Gao, Yu-Jie Wang, Shun-Li Li, Ya-Qian Lan *

Jiangsu Collaborative Innovation Centre of Biomedical Functional Materials, Jiangsu Key Laboratory of New Power Batteries, School of Chemistry and Materials Science, Nanjing Normal University, Nanjing 210023, China

ARTICLE INFO

Article history:
Received 3 April 2020
Received in revised form 22 April 2020
Accepted 11 May 2020
Available online 15 May 2020

Keywords:
Chloroplast-like porous structure
Bi-based activated metastable layer
CO_2 electroreduction
High energy efficiency
Formate

ABSTRACT

Electrochemical CO_2 reduction reaction (CO_2RR) to formate is economically viable considering the energy input and market value. Through learning nature, a series of chloroplast-like porous bismuth-based core–shell (CPBC) materials have been designed. In these materials, the porous carbon can enrich and transfer CO_2 to the core–shell Bi@Bi_2O_3 in CO_2 reduction process, during which Bi_2O_3 layer can be transformed into activated metastable layer to efficiently convert CO_2 into formate and Bi can provide abundant electrons. Based on this, superior performances for most of important parameters in CO_2RR can be achieved and best of them, CPBC-1 presents remarkable Faradaic efficiency ($FE_{formate}$ > 94%) over a wide potential range (−0.65 to −1.0 V) with high catalysis durability (>72 h). Noteworthy, its maximum energy efficiency is as high as 76.7% at −0.7 V, the highest one in reported bismuth-based materials. This work opens novel perspectives in designing nature-inspired CO_2RR electrocatalysts.

1. Introduction

The anthropic excessive emission of CO_2 has resulted in serious environmental issues and energy crisis [1,2]. By using renewable electricity as the driving force, electrochemical CO_2 reduction reaction (CO_2RR) that can convert CO_2 into value-added fuels or chemicals has aroused to be a promising pathway to fix CO_2 [3–9]. However, the adsorption and activation process of CO_2 reduction still needs high energy due to its intrinsically chemical inertness accompanied with the competitive hydrogen evolution reaction (HER), which generally results in low activity and selectivity [10–13]. Chloroplast, the most vital and common plastid in plant cells, can enrich, fix and convert CO_2 into carbohydrates using energy, which is essential for the maintenance of life on earth [14–16]. To address the problems of CO_2RR and imitate nature, the design of highly stable and efficient electrocatalysts with chloroplast-like structure might be alternative strategy to enrich and convert CO_2 into valuable products in CO_2RR [17].

In electrochemical CO_2RR, formate is a kind of economically viable product and has been widely used in diverse applications such as feedstock in pharmaceutical or textile industry, hydrogen carrier for fuel cell [18–21]. Electroreduction of CO_2 into formate through mild and energy-favored approach has been intensively investigated, yet the performance target for practical applications (minimum current density (j) required is ~ 200 mA cm^{-2}, Faradaic efficiency (FE) > 95% and catalyst durability > 1000 h) still remains giant challenge to bring any electrocatalyst materials from experiment scale to industrial scale implementation [22,23]. Until now, many materials have been devoted in the CO_2RR to formate [24,25], such as Bi- [26–30], In- [31,32] or Sn- [33–35] based electrocatalysts. Unfortunately, there are still some inevitable bottlenecks like: (1) most of materials only show moderate performances in one or two important parameters (e.g., FE, potential range, stability, current density or energy efficiency (EE)), which is far from meeting the performance target for practical applications; (2) the adsorption and enrichment ability of CO_2 on catalyst, which is vital and key step during CO_2RR process and (3) electron or proton migration ability that can determine the generation of intermediate products. Therefore, the design of powerful electrocatalysts with high porosity, well-tuned morphology and remarkable activity that can meet most of important parameters essential for practical applications is demanded. Through learning nature, chloroplast-inspired materials with structures like envelope in chloroplast that can enrich, diffuse and transfer CO_2 to active centers and further convert CO_2 into valuable products in an integrated system to simulate chloroplast might be promising alternatives for electrochemical CO_2RR.

* Corresponding authors.
E-mail addresses: chyf927821@163.com (Y. Chen), yqlan@njnu.edu.cn (Y.-Q. Lan).
[1] These authors contributed equally to this work.

https://doi.org/10.1016/j.scib.2020.05.010
2095-9273/

Taking these considerations in mind, we focus on the construction of powerful Bi-based electrocatalysts with porous structure for highly selective CO_2RR. Herein, we have successfully synthesized a series of Bi-MOF derived materials (CPBC-*x*, *x* = 1, 2, 3, 4) with chloroplast-like porous core–shell structure (Fig. 1a). The porous carbon could serve as the function like envelope in chloroplast to capture, enrich and transfer CO_2 and core–shell Bi@Bi_2O_3 nanoparticles would act as the active sites. The integration of them can provide abundant active sites, reduce contact resistance and efficient mass transfer in CO_2RR. Specially, CPBC-1 exhibits high $FE_{formate}$ (>94%) over a wide potential range (−0.65 to −1.0 V) and excellent catalysis stability (>72 h). It also presents a maximum EE of 76.7% at −0.7 V, which is the highest one among Bi-based electocatalysts.

2. Material and methods

2.1. Synthesis of Bi-MOF and the preparation of CPBC-x

Bi-MOF was prepared following the previously reported method with slight modification [36]. $Bi(NO_3)_2{\cdot}5H_2O$ (0.15 g, 0.38 mmol) and H_3BTC (0.75 g, 3.5 mmol) were dissolved in 60 mL methanol under stirring. Subsequently, the solution was transferred into a 100 mL Teflon reactor to heat at 120 °C for 24 h. The resulting precipitate was collected by centrifugation and washed with methanol for several times. After drying at 60 °C for 24 h, Bi-MOF was obtained for further characterization.

The preparation of CPBC-*x* is achieved through the heat-treating of obtained Bi-MOF. Taking CPBC-1 for example, the Bi-MOF powder was placed into a tubular furnace and heat-treated in the presence of N_2 atmosphere at 400 °C for 1 h (the heating rate is 5 °C min^{-1}). As comparison, CPBC-*x* (*x* stands for the temperature) treated at different temperature (500–800 °C) were also synthesized followed the similar procedures (CPBC-1, 400 °C; CPBC-2, 500 °C; CPBC-3, 600 °C and CPBC-4, 800 °C).

2.2. Synthesis of carbonized precursors

$Bi(NO_3)_2{\cdot}5H_2O$ (0.15 g, 0.38 mmol) and H_3BTC (0.75 g, 3.5 mmol) were grounded 30 min to form uniformly mixture. Then the mixture power was placed into a tubular furnace and heat-treated in the presence of N_2 atmosphere at 400 °C for 1 h (the heating rate is 5 °C min^{-1}).

2.3. Material characterization

Powder X-Ray diffraction (PXRD) patterns of samples were recorded on a D/max 2500 VL/PC diffractometer (Japan) equipped with Cu Kα radiation (λ = 1.54060 Å) at 40 kV and 100 mA. Raman spectra of powder samples were obtained on Lab-RAM HR800 with a laser excitation wavelength of 633 nm. N_2 adsorption–desorption isotherms were determined by Micromeritics ASAP 2460 system at 77 K. Before the measurement, the catalysts were degassed at 120 °C for 12 h. Scanning electron microscopy (SEM) and energy-dispersive X-ray spectroscopy (EDS) of samples were analyzed by SEM (JEOL JSM-7600F) with acceleration voltage of 10 and 15 kV, respectively. Transmission electron microscopy (TEM) images, high-resolution TEM (HRTEM) images and STEM-HAADF images coupled to EDS elemental mapping were collected on a JEOL JEM-2100 electron microscope at 200 kV equipped with an Oxford Energy dispersive X-ray spectroscopy. X-ray photoelectron spectroscopy (XPS) was collected on a Thermo ESCALAB 250XI multifunctional imaging electron spectrometer using the binding energy of C as the internal standard.

2.4. Electrochemical measurements

All electrochemical measurements of the samples were measured on the Bio-Logic VSP electrochemical workstation in 0.5 mol L^{-1} $KHCO_3$. The carbon paper (1 cm × 2 cm), carbon rod and Ag/AgCl electrode were used as the working, counter and reference electrode, respectively. The experiment was performed in the H-type cell, two compartments were separated by an exchange membrane (Nafion®117). The preparation of the working electrode was given as follows. 10 mg electrocatalyst and 5 mg acetylene black were grounded, then 1 mL 0.5% Nafion solution were added into the mixture and treated by sonication to form uniform catalyst ink. After sonication for 30 min, the ink was dropped directly onto a carbon paper (1 cm × 1 cm) with a catalyst loading density of ~1 mg cm^{-2} and dried.

During the CO_2 reduction experiments, the linear sweep voltammetry (LSV) was measured at a scan rate of 5 mV s^{-1}. Initially, LSV was recorded under an inert N_2 (gas) saturated 0.5 mol L^{-1} $KHCO_3$ (pH 8.8). After that, the solution was bubbled with CO_2 (99.999%) for at least 30 min to make the electrolyte saturated (pH 7.2) and then carry out the electrocatalytic CO_2RR. The potentials in this work were tested versus Ag/AgCl electrode and reported versus reversible hydrogen electrode (RHE) based on the Nernst equation: E (vs. RHE) = E (vs. Ag/AgCl) + 0.1989 + 0.059 × pH. Electrochemical impedance spectroscopy (EIS) measurement was performed in a frequency range from 1000 kHz to 0.1 Hz by applying an AC voltage with 10 mV amplitude at −0.7 V (vs. RHE). To estimate the electrochemical active surface area (ECSA), cyclic voltammograms (CV) were tested by measuring double-layer capacitance (C_{dl}) under the potential window of 0.00–0.10 V (vs. Ag/AgCl) with various scan rates from 10 to 200 mV s^{-1}. All the electrochemical measurements were performed without iR compensation.

2.5. Reaction product analysis

The electrochemical measurements were carried out at selected potentials (−0.5 to −1 V) to determine the reduction products and their Faradaic efficiency. The CO was monitored by a gas chromatography (GC-7920) equipped with a flame ionization detector (FID). A thermal conductivity detector (TCD) was used to analyze hydrogen. The liquid products (e.g., formate) were collected from the cathode chambers after electrolysis and quantified by ion chromatography (IC).

3. Results and discussion

3.1. Structural and morphological characterization

The preparation of chloroplast-like materials are obtained from hydrothermal method coupled with heat-treating (see the Experimental Section in the Supplementary materials, Fig. S1 online) [36]. Taking the CPBC-1 for example, the inherent structure of Bi-MOF is transferred into a mixed phase of Bi (JCPDS No. 1–699) and Bi_2O_3 (JCPDS No. 27–50) as proved by the PXRD tests after heat-treating (400 °C) (Fig. 1b). To evaluate the porosity of the materials, N_2 sorption tests are conducted. CPBC-1 exhibits a Brunauer-Emmett-Teller surface area (S_{BET}) of 194 m^2 g^{-1}, slightly lower than that of Bi-MOF (297 m^2 g^{-1}) (Table S1 online) [37]. Interestingly, the pore size distribution of CPBC-1 demonstrates two kinds of micropores (0.87 and 1.18 nm), which implies the remained porosity after heat treating (Fig. S2 online). Besides, to evaluate the superiority of these highly porous materials, the CO_2 temperature programmed desorption (CO_2-TPD) test is conducted. These materials show broad and intense desorption peaks in the ranges of 300–500 °C, which are attributed to the moderate or

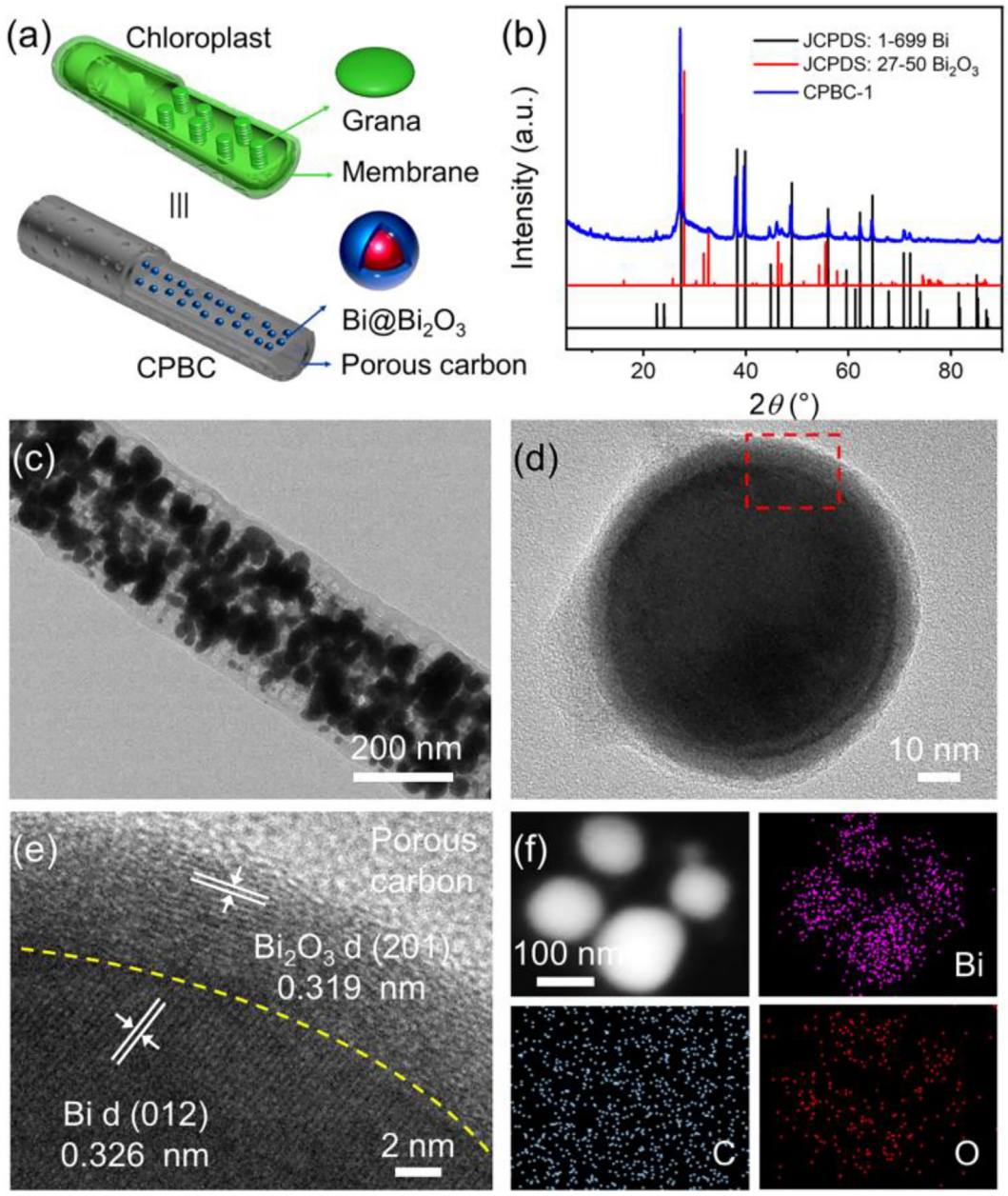

Fig. 1. (Color online) Characterization of CPBC-1. (a) Schematic illustration of chloroplast-like structure. (b) PXRD patterns. (c) TEM image of the chloroplast-like structure. (d) TEM image of the core–shell structure. (e) HRTEM image in (d). (f) STEM and mapping images.

strong basic sites [38–40]. The amounts of adsorbed CO_2 on these chloroplast-like materials show much stronger basicity than commercial Bi and Bi_2O_3 (Fig. S3 and Table S2 online). Specially, CPBC-1 (0.41 mmol g^{-1}) exhibits ~8 and ~4 times adsorption capacity of CO_2 larger than commercial Bi (0.05 mmol g^{-1}) and Bi_2O_3 (0.1 mmol g^{-1}), respectively, indicating the structure superiority of these porous chloroplast-like materials. The existence of Bi (73 and 3073 cm^{-1}) and Bi_2O_3 (91, 100 and 315 cm^{-1}) can be further detected in the Raman test (Fig. S4 online). Besides, the peaks at 1305 and 1589 cm^{-1} are assigned to the D and G band of carbon materials, respectively.

In order to detect the morphology of the relevant materials, SEM and TEM tests are performed. As shown in SEM images, Bi-MOF displays a rod-like morphology (length, ~13 μm and width, ~2 μm) (Fig. S5 online). After heat-treating, the rod-like morphology can be maintained while the size is slightly shrunk (length, ~13 μm and width, ~1.5 μm) (Fig. S6 online). Specially, a kind of chloroplast-like porous structure is detected in the TEM image of CPBC-1. In the structure, large amount of nanoparticles are uniformly distributed in the porous carbon and the nanoparticles possess core–shell structures with diameter about 80 nm (Fig. 1c). The grain boundary of Bi and Bi_2O_3 is observed in the HRTEM test, in which Bi serves as the core (diameter, ~74 nm) and Bi_2O_3 as the shell (thickness, ~4 nm) (Figs. 1d and S7 online). In the core–shell structure, the lattice spacings of 0.326 and 0.319 nm are ascribed to (0 1 2) and (2 0 1) planes of Bi and Bi_2O_3, respectively (Fig. 1e). The core–shell structure is further certified by the linear scanning of EDX spectrometry, in which the O is first detected and the thickness of Bi_2O_3 matches well with the TEM result (Figs. S8 and S9 online). Moreover, the high-angle annular dark-field scanning transmission electron microscopy (HAADF-STEM) image and the corresponding element mapping of CPBC-1 show that Bi element is concentrated in the nanoparticle area while C element is uniformly distributed in the whole sample (Figs. 1f

and S10 online). All these results suggest that CPBC-1 has a special chloroplast-like morphology, in which uniformly distributed Bi@Bi_2O_3 core–shell nanoparticles like grana or stroma and porous carbon might act as the function of chloroplast envelope.

XPS characterization is further performed to analyze the electronic state on the surface of the CPBC-1 (Fig. S11a online). The high-resolution XPS spectrum of Bi 4f exhibits two different valence states. The binding energies at 164.3 and 159 eV are ascribed to Bi^{3+} $4f_{5/2}$ and $4f_{7/2}$, while two peaks at 162.6 and 157.2 eV are assigned to Bi $4f_{5/2}$ and $4f_{7/2}$, indicating the successful preparation of Bi@Bi_2O_3 (Fig. S11b online) [41–43]. The O 1s spectrum shows three peaks including Bi–O (529.8 eV), C=O (530.7 eV) and C–OH (531.9 eV) (Fig. S11c online) [44]. The C 1s can be deconvoluted into a strong peak of C–C/C=C at 284.6 eV and two relatively weak peaks of C–O at 285.9 eV and O–C=O at 289 eV, respectively, which suggests the existence of porous carbon in CPBC-1 (Fig. S11d online) [45].

Except for CPBC-1, different treating temperatures (500 °C, CPBC-2; 600 °C, CPBC-3 and 800 °C, CPBC-4) are further investigated. The main compositions of the samples are Bi and Bi_2O_3 as proved by the PXRD tests (Fig. S12 online). Different morphologies are observed in the SEM and TEM images (Fig. S6 online and Fig. 2a–c). In these materials, the particle distribution density changes from loose to dense and the thickness of Bi_2O_3 shell in the structure becomes larger and larger with the increase of temperature. The average shell thickness of CPBC-2, CPBC-3 and CPBC-4 are detected to be 7.1, 9.3 and 14.3 nm, respectively (Fig. 2d–i). Besides, the diameter of the core displays a decreased curve with the temperature increasing from 400 to 800 °C (i.e., CPBC-1, (73.8 ± 3.0) nm; CPBC-2, (68.0 ± 3.6) nm; CPBC-3, (69.0 ± 4.1) nm and CPBC-4, (44.8 ± 3.8) nm) (Figs. 1d and 2d–f). The porosity of these materials is further characterized by N_2 sorption tests (Fig. S13 online). The S_{BET} values of CPBC-2, CPBC-3 and CPBC-4 are calculated to be 86, 116 and 115 $m^2\ g^{-1}$, respectively (Table S1 online). In addition, XPS tests of these materials are further conducted to study the electronic states. The intensity of peaks at 162.6 and 157.2 eV (attributed to Bi) are gradually decreased with the increase of temperature, demonstrating the enhancement of thickness for Bi_2O_3 shell (Figs. S14–S16 online).

3.2. Electrocatalytic performance

The specially designed chloroplast-like materials with highly porous structure might serve as powerful electrocatalysts for electrochemical CO_2RR. LSV curves show that the CO_2RR polarization curve of CPBC-1 abruptly takes off at about –0.6 V, increases shar-

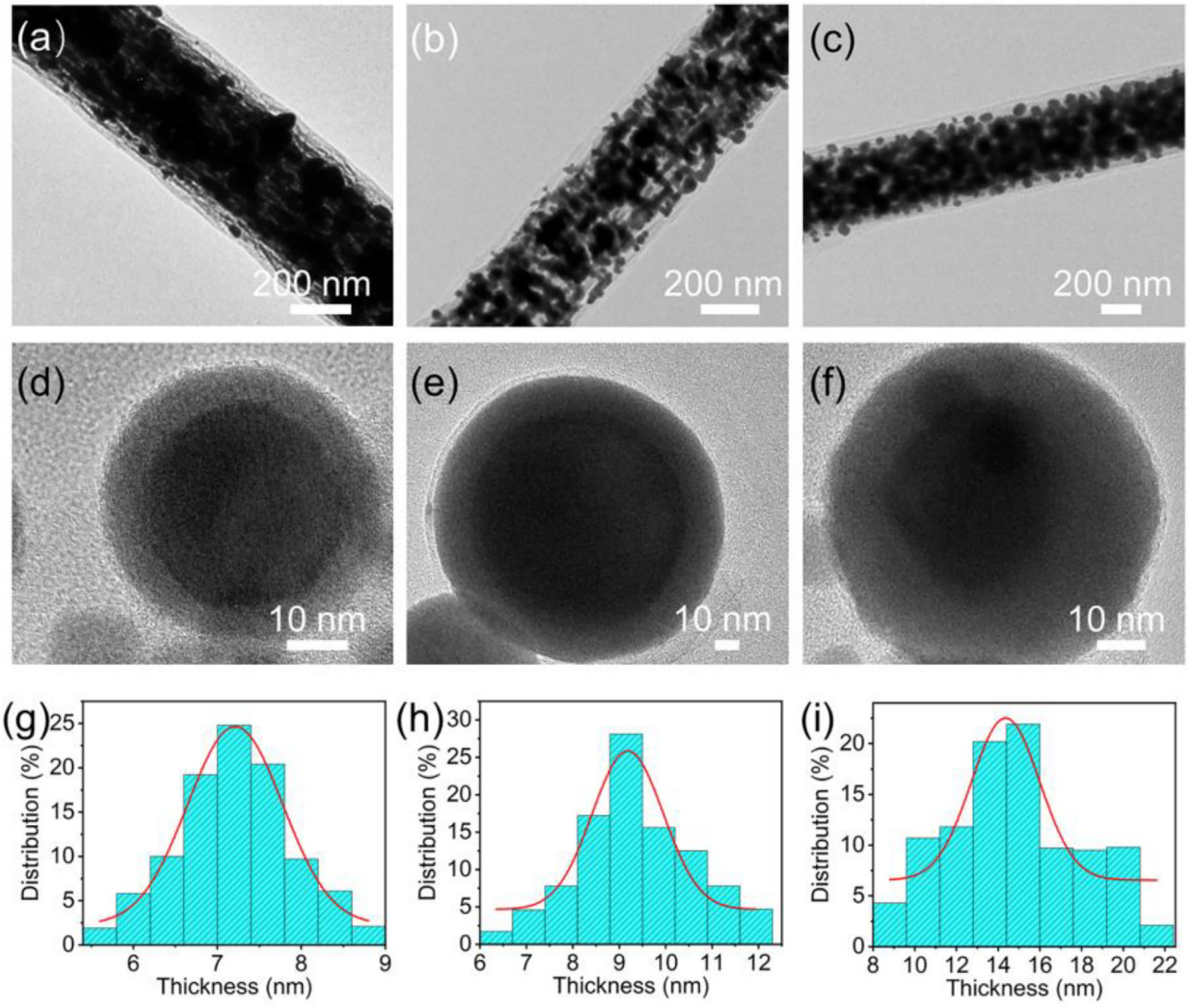

Fig. 2. (Color online) Characterization of CPBC-2, CPBC-3 and CPBC-4. (a–c) TEM images. (d–f) HRTEM images. (g–i) The thickness distribution of Bi_2O_3 shell (the thickness of Bi_2O_3 shell is calculated based on the Nano-measurer software).

ply and reaches to –24.4 mA cm^{-2} at –1.0 V. CPBC-1 has much smaller current density in HER than that in CO_2RR, indicating CPBC-1 strongly favors CO_2RR over HER (Fig. S17 online). To reveal superiority of the materials, samples including commercial Bi, commercial Bi_2O_3, carbonized precursors and physical mixture (Bi and Bi_2O_3) are prepared and measured as comparisons (Figs. S18–S20 online). The current density of CPBC-1 is higher than Bi (–10.8 mA cm^{-2}), Bi_2O_3 (–10.5 mA cm^{-2}), carbonized precursors (–9.2 mA cm^{-2}) and physical mixture (–12.9 mA cm^{-2}) (Fig. 3a). In order to detect the reduction product, the electrolysis is performed at different potentials. The gas and liquid products are monitored by gas chromatography and IC tests, respectively (Fig. S21 online). As a result, the formate is found to be the dominant product accompanied by the co-generation of a small amount of CO and H_2 (Fig. S22 online). For CPBC-1, the initial formation of formate is detected at overpotential of 150 mV with a small $FE_{formate}$ of 2.8%. With the increase of potential, the $FE_{formate}$ continuously increases and reaches up to ~100% at −0.7 V and keeps higher than 94% over a wide potential range from −0.65 to −1.0 V (Fig. 3b and Fig. S23 online). Noteworthy, as far as we known, the ultrahigh formate selectivity over such a broad potential window is far superior to most of formate-producing CO_2RR electrocatalysts (e.g., Sn, In and N-doped carbon, etc.) [15,27,28,35]. The excellent performance (−0.65 to −1.0 V, $FE_{formate}$ > 94%) also surpasses most of Bi-based materials, thereby unambiguously underlining the unique advantages of CPBC-1 with chloroplast-like structure (Table S3 online) [26,29].

In contrast, Bi only displays moderate performances over relatively narrow potential range (Fig. 3b). The $FE_{formate}$ of Bi can only reach above 90% in narrow potential range similar as many reported Bi-based electrocatalysts [26], which is far inferior to CPBC-1 (Fig. 3b). The similar phenomenon is detected for Bi_2O_3 (33%, −0.9 V), carbonized precursors (83%, −1.0 V) and physical mixture (95%, −1.0 V). To further reveal the activity of CPBC-1, partial current density of formate is calculated (Fig. 3c). CPBC-1 displays a high value of −22.9 mA cm^{-2} at −1.0 V, which is almost 10, 4, 3 and 2 times than those of Bi (−2.4 mA cm^{-2}), Bi_2O_3 (−6.0 mA cm^{-2}), carbonized precursors (−7.7 mA cm^{-2}) and physical mixture (−12.4 mA cm^{-2}), respectively. The superior performance of CPBC-1 indicates the advantage of chloroplast-like porous structures in electrochemical CO_2RR. To further support the superiority of the structure, we directly transfer CPBC-1 into material with only Bi_2O_3- (carbonized under air at 400 °C) or Bi- (HCl etched and cathodically converted at −0.9 V) based materials

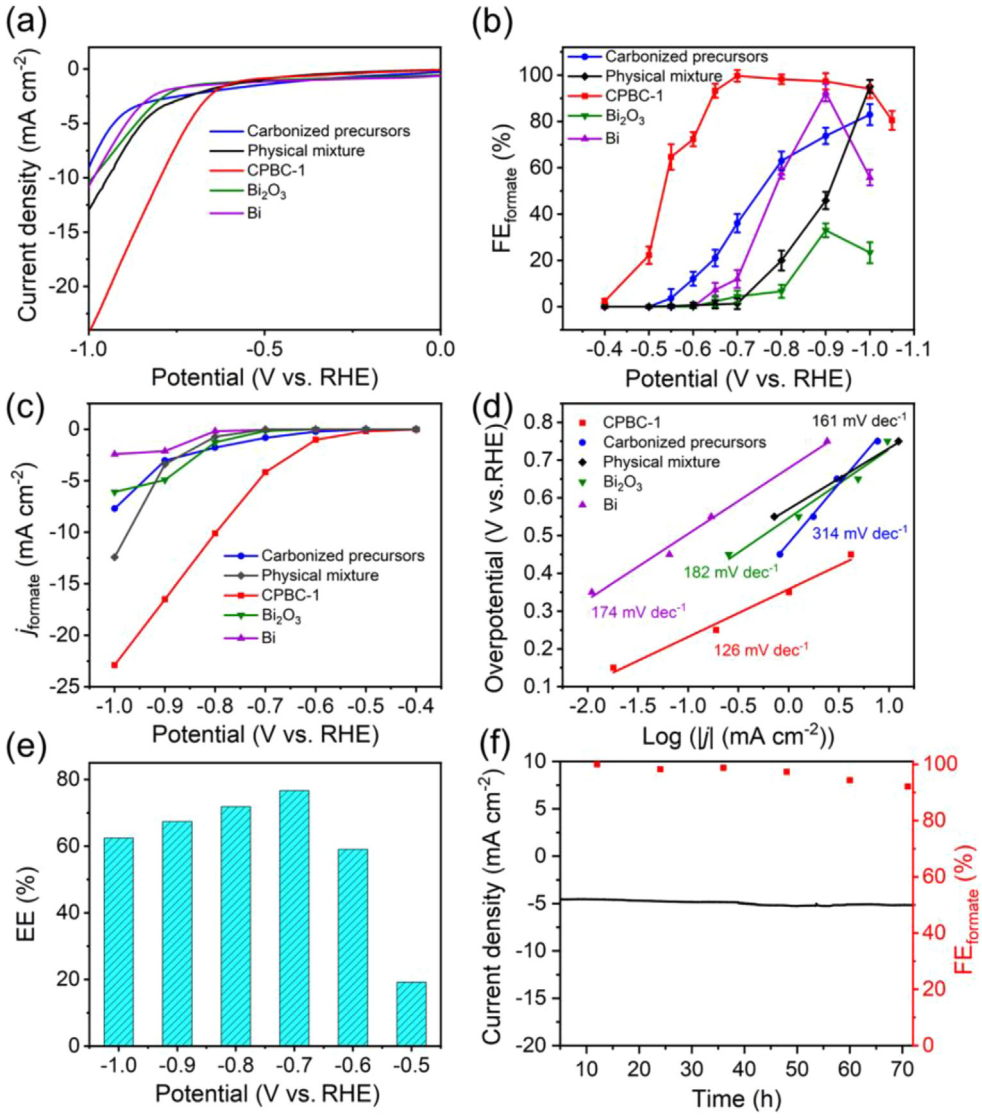

Fig. 3. (Color online) Electrocatalytic performances of CPBC-1, Bi, Bi_2O_3, carbonized precursors and physical mixture. (a) Linear sweep voltammetric curves. (b) Faradaic efficiency for formate. (c) Partial current density for formate. (d) Tafel plots. (e) Energy efficiency of CPBC-1. (f) Durability test of CPBC-1 at the potential of −0.7 V (vs. RHE).

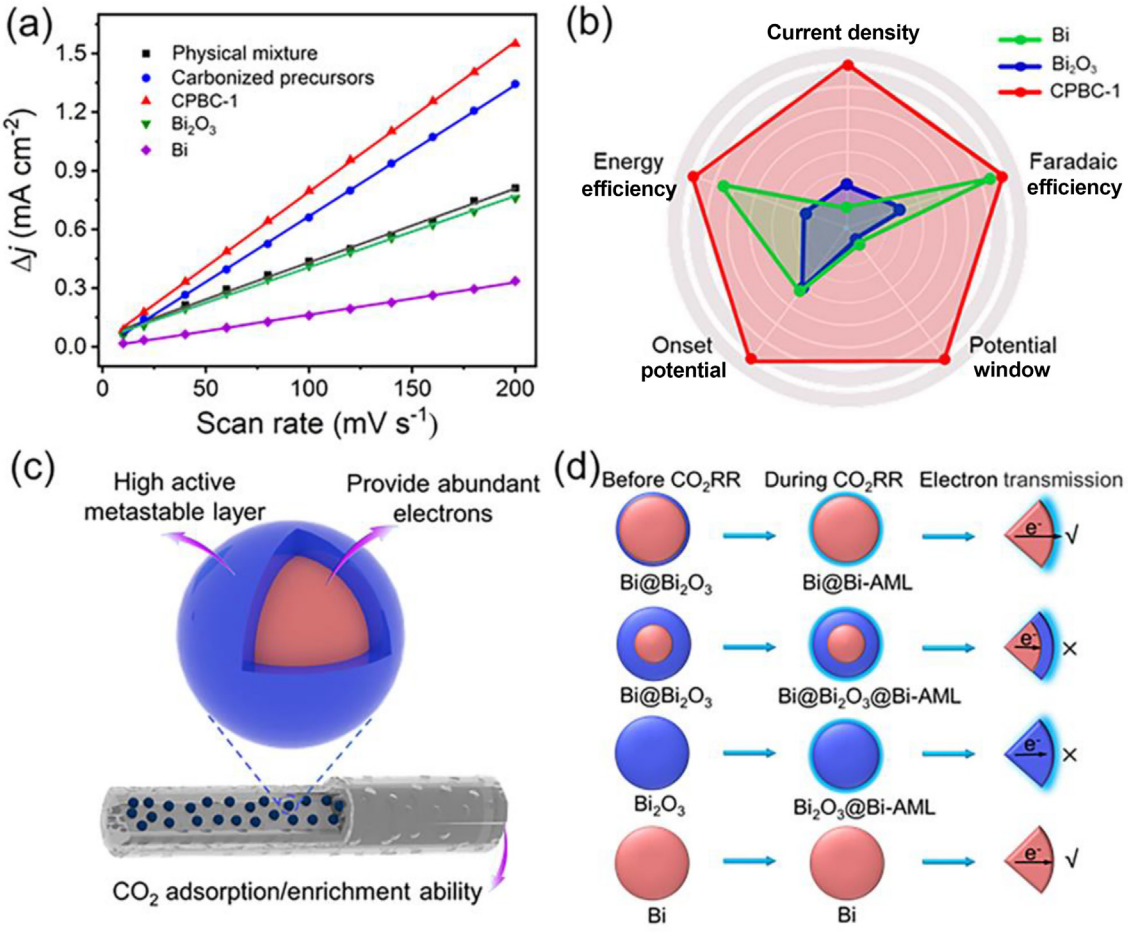

Fig. 4. (Color online) The performances and possible electrocatalysis mechanism of CPBC-1 and its contrast samples. (a) Electrochemical double-layer capacitance. (b) Radar chart of the performances for Bi, Bi_2O_3 and CPBC-1. (c) Schematic illustration of the function for chloroplast-like structure in electrocatalysis. (d) Representative core–shell structures and their possibility in electron transfer (Bi-AML stands for Bi-based activated metastable layer).

as proved by the PXRD tests (Fig. S24 online). After heat-treating, only Bi_2O_3-based material displays a $FE_{formate}$ of 81% at −1.0 V, which is much lower than that of CPBC-1 (Fig. S25 online). Similar result is also detected in only Bi-based material, in which the $FE_{formate}$ only displays 41% at −1.0 V (Fig. S26 online). Moreover, to reveal the connection between the activity and Bi_2O_3 shell1845 thickness, the electroreduction properties of CPBC-2, CPBC-3 and CPBC-4 are tested (Fig. S27 online). The highest $FE_{formate}$ for CPBC-2, CPBC-3 and CPBC-4 are achieved at −0.9 V (92%), −1.0 V (99%) and −0.8 V (62%), respectively. However, CPBC-2, CPBC-3 and CPBC-4 all possess narrower potential range for the high $FE_{formate}$ and larger overpotential coupling with the declined $FE_{formate}$ compared with CPBC-1. Tafel slopes are calculated to further confirm the reaction kinetics for the formate formation (Fig. 3d). Notably, the Tafel slope of CPBC-1 is 126 mV dec^{-1}, which is lower than that of Bi (174 mV dec^{-1}), Bi_2O_3 (182 mV dec^{-1}), carbonized precursors (314 mV dec^{-1}) and physical mixture (161 mV dec^{-1}), suggesting the enhanced CO_2RR kinetic. Moreover, the EE of CPBC-1 is calculated to estimate the energy conversion efficiency in the CO_2RR process (Fig. 3e). The high $FE_{formate}$ together with the low overpotential of CPBC-1 contributes to the large EE (>50%) in a wide potential window (−0.55 to −1.05 V) and a maximum value of 76.7% is achieved at −0.7 V, which is the highest among Bi-based CO_2RR electrocatalysts (Table S4 online) [18,46–49].

To analyze the electrochemical stability of CPBC-1, longtime durability test is carried out at an overpotential of 450 mV by chronoamperometric test (Fig. 3f). During the process, the $FE_{formate}$ can be maintained at values>92% for 72 h. The PXRD results prove the CPBC-1 can remain stable during the longtime durability test (Fig. S28 online). The result reveals that CPBC-1 is a kind of stable electrocatalyst, which has much potential to be used in efficient electrochemical CO_2RR. Moreover, the electrochemical double-layer capacitance (C_{dl}) is detected and CPBC-1 gives a larger C_{dl} value (7.69 mF cm^{-2}) than Bi (3.64 mF cm^{-2}), Bi_2O_3 (1.66 mF cm^{-2}), and physical mixture (3.78 mF cm^{-2}), which suggests that CPBC-1 might offer more active sites to contact the electrolyte (Fig. 4a and Fig. S29 online). In addition, the charge transfer resistance of CPBC-1, Bi, Bi_2O_3, carbonized precursors and physical mixture are calculated to be 16.6, 115.3, 85.2, 47.7 and 131.7 Ω, respectively, confirming faster electron transfer efficiency for CPBC-1 (Fig. S31 online).

The high stability coupling with well-tuned morphology imparts these materials with excellent electrocatalysis performances (Fig. 4b). Based on the experimental results, we made a radar chart of the performances for Bi, Bi_2O_3 and CPBC-1. As shown in Fig. 4b, CPBC-1 has broader potential window (−0.65 to −1.0 V, $FE_{formate}$ > 94%) and higher FE (−0.7 V, ~100%) than Bi (−0.9 V, 33%) or Bi_2O_3 (−0.9 V, 33%). Besides, CPBC-1 displays a high value of −22.9 mA cm^{-2} at −1.0 V, which is almost 10, 4 times than those of Bi (−2.4 mA cm^{-2}) and Bi_2O_3 (−6.0 mA cm^{-2}), respectively. These results indicate the superior performances of CPBC-1 over other comparisons. We intend to briefly reveal the superiority of the chloroplast-like porous core–shell structure. Some previous works display that the oxide layer on the surface of metal catalyst is beneficial for CO_2RR [46,49,50]. In the CO_2RR process, the Bi-

based oxide layer might transfer into Bi-based activated metastable layer (Bi-AML) that can serve as active catalysis center in CO_2RR (Fig. 4c). Here, we propose four types of structures based on the thickness of Bi_2O_3 shell and discuss their mechanism in CO_2-RR (Fig. 4d). For the first type of Bi@Bi_2O_3 with moderate shell thickness, the Bi_2O_3 shell can be rapidly and completely converted into Bi-AML and the inner Bi layer can give sufficient electrons to facilitate the efficient CO_2RR process under voltage condition. As proved by the CO_2RR performance, CPBC-1 with similar structure exhibits excellent electrocatalytic performance ($FE_{formate}$, ~100% at −0.7 V) (Figs. 4d and 3b). In contrast, if the thickness of Bi_2O_3 shell is too thick, the Bi_2O_3 cannot be completely transferred into Bi-AML under voltage condition, thus leading to a possible three-layer state and presents relatively low performance since the middle Bi_2O_3 layer might block the electron transfer pathway (Fig. 4d). This matches well with the poor performances of CPBC-2 ($FE_{formate}$, 92% at −0.9 V), CPBC-3 ($FE_{formate}$, 99% at −1.0 V) and CPBC-4 ($FE_{formate}$, 62% at −0.8 V). For the third type of pure Bi_2O_3, the inner Bi_2O_3 is hard to provide sufficient electrons to the Bi-AML and the properties including FE and potential range are far inferior to the first type with suitable shell thickness, which are supported by the poorer performances of commercial Bi_2O_3 and air-treated CPBC-1 (Fig. 4d). Finally, for the fourth type of pure Bi with inevitable and thimbleful Bi_2O_3 layer on the surface, the insufficient Bi-AML under voltage condition results in decreased activity (e.g., relatively lower $FE_{formate}$ and narrower potential range for high $FE_{formate}$) of commercial Bi compared to the first type with moderate shell thickness (Fig. 4d).

Based on the experimental results, we propose a possible electrochemical CO_2RR mechanism to better understand the catalysis process. In the electrochemical CO_2RR process, CO_2 is firstly adsorbed and enriched in the porous structure and efficiently transferred to the core–shell active centers. Meanwhile, the Bi_2O_3 shell of Bi@Bi_2O_3 rapidly and completely converts into Bi-AML under voltage condition. Then the adsorbed CO_2 accepts an electron (from working electrode) and an H^+ (from electrolyte) to generate OCHO* intermediate. Subsequently, OCHO* converts to formate coupling with the proton-electron transfer. Finally, the produced formate is quickly desorbed from the catalysts surface and efficiently transferred into electrolyte to finish the catalysis process.

4. Conclusions

In summary, we have successfully synthesized a series of materials with chloroplast-like porous core–shell structure. In these materials, the porous carbon can enrich and transfer CO_2 to the core–shell Bi@Bi_2O_3 centers in CO_2RR process, during which Bi_2O_3 layer can be transformed into activated metastable layer to efficiently convert CO_2 into formate and Bi can provide abundant electrons. Specially, CPBC-1 enables to selectively convert CO_2 into formate with an excellent $FE_{formate}$ of ~100% and remarkable catalysis stability (>72 h). Particularly, CPBC-1 exhibits large EE (>50%) in a wide potential window (−0.55 to −1.05 V) and a maximum value of 76.7% is achieved at −0.7 V, which is the highest in Bi-based CO_2RR electrocatalysts. The remarkable performances are associated with its unique superstructure, having simultaneous CO_2 adsorption or enrichment ability, abundant active sites and fast electron–proton transfer efficiency with significant synergetic effects in efficient CO_2RR electrocatalysis. This work might shed light on the exploration of nature-inspired and robust electrocatalysts to address CO_2 problems.

Conflict of interest

The authors declare that they have no conflict of interest.

Acknowledgments

This work was financially supported by the National Natural Science Foundation of China (21622104, 21871142 and 21901122), the Natural Science Foundation of Jiangsu Province of China (BK20171032), the Natural Science Research of Jiangsu Higher Education Institutions of China (17KJB150025 and 19KJB150011) and Projects funded by China Postdoctoral Science Foundation (2018 M630572 and 2019 M651873), Priority Academic Program Development of Jiangsu Higher Education Institutions and the Foundation of Jiangsu Collaborative Innovation Center of Biomedical Functional Materials.

Author contributions

Ya-Qian Lan and Yi-Rong Wang conceived the idea. Yi-Rong Wang designed the experiments, collected and analyzed the data. Yi-Rong Wang and Ru-Xin Yang carried out the experiments. Guang-Kuo Gao and Yu-Jie Wang assisted with the characterizations. Yi-Rong Wang wrote the manuscript. Shun-Li Li, Yifa Chen and Ya-Qian Lan commented on the manuscript.

Appendix A. Supplementary materials

Supplementary materials to this article can be found online at https://doi.org/10.1016/j.scib.2020.05.010.

References

[1] Shakun JD, Clark PU, He F, et al. Global warming preceded by increasing carbon dioxide concentrations during the last deglaciation. Nature 2012;484:49–54.
[2] Dowell NM, Fennell PS, Shah N, et al. The role of CO_2 capture and utilization in mitigating climate change. Nat Clim Change 2017;7:243–9.
[3] Kim D, Xie C, Becknell N, et al. Electrochemical activation of CO_2 through atomic ordering transformations of AuCu nanoparticles. J Am Chem Soc 2017;139:8329–36.
[4] Li J, Chen G, Zhu Y, et al. Efficient electrocatalytic CO_2 reduction on a three-phase interface. Nat Catal 2018;1:592–600.
[5] Mou S, Wu T, Xie J, et al. Boron phosphide nanoparticles: a nonmetal catalyst for high-selectivity electrochemical reduction of CO_2 to CH_3OH. Adv Mater 2019;31:1903499.
[6] Wang Y-R, Huang Q, He CT, et al. Oriented electron transmission in polyoxometalate-metalloporphyrin organic framework for highly selective electroreduction of CO_2. Nat Commun 2018;9:4466.
[7] Dinh CT, Burdyny T, Kibria MG, et al. CO_2 electroreduction to ethylene via hydroxide-mediated copper catalysis at an abrupt interface. Science 2018;360:783–7.
[8] Fu J, Zhu W, Chen Y, et al. Bipyridine-assisted assembly of Au nanoparticles on Cu nanowires to enhance electrochemical reduction of CO_2. Angew Chem Int Ed 2019;58:14100–3.
[9] Jiao J, Lin R, Liu S, et al. Copper atom-pair catalyst anchored on alloy nanowires for selective and efficient electrochemical reduction of CO_2. Nat Chem 2019;11:222–8.
[10] Nitopi S, Bertheussen E, Scott SB, et al. Progress and perspectives of electrochemical CO_2 reduction on copper in aqueous electrolyte. Chem Rev 2019;119:7610–72.
[11] Gu Z, Shen H, Shang L, et al. Nanostructured copper-based electrocatalysts for CO_2 reduction. Small Methods 2018;2:1800121.
[12] Sun ZY, Ma T, Tao HC, et al. Fundamentals and challenges of electrochemical CO_2 reduction using two-dimensional materials. Chem 2017;3:560–87.
[13] Birdja YY, Pérez-Gallent E, Figueiredo MC, et al. Advances and challenges in understanding the electrocatalytic conversion of carbon dioxide to fuels. Nat Energy 2019;4:732–45.
[14] Heijne G, Von Steppuhn J, Herrmann RG. Domain structure of mitochondrial and chloroplast targeting peptides. Eur J Biochem 2010;180:535–45.
[15] Maione TE, Gibbs M. Hydrogenase-mediated activities in isolated chloroplasts of chlamydomonas reinhardii. Plant Physiol 1986;80:360–3.
[16] Olmstead RG, Palmer JD. Chloroplast DNA systematics: a review of methods and data analysis. Am J Bot 1994;81:1205–24.
[17] Zheng Y, Vasileff A, Zhou X, et al. Understanding the roadmap for electrochemical reduction of CO_2 to multi-carbon oxygenates and hydrocarbons on copper-based catalysts. J Am Chem Soc 2019;141:7646–59.
[18] Liu S, Lu XF, Xiao J, et al. Bi_2O_3 nanosheets grown on multi-channel carbon matrix to catalyze efficient CO_2 electroreduction to HCOOH. Angew Chem Int Ed 2019;58:13828–33.

[19] Agarwal AS, Zhai Y, Hill D, et al. The electrochemical reduction of carbon dioxide to formate/formic acid: engineering and economic feasibility. ChemSusChem 2011;4:1705.
[20] Zhang Y, Zhang X, Ling Y, et al. Controllable synthesis of few-layer bismuth subcarbonate by electrochemical exfoliation for enhanced CO_2 reduction performance. Angew Chem Int Ed 2018;130:13467–71.
[21] Kibria MG, Edwards JP, Gabardo CM, et al. Electrochemical CO_2 reduction into chemical feedstocks: from mechanistic electrocatalysis models to system design. Adv Mater 2019;31:1807166.
[22] Verma S, Kim B, Jhong HM, et al. A gross-margin model for defining technoeconomic benchmarks in the electroreduction of CO_2. ChemSusChem 2016;9:1972–9.
[23] Atifi A, Boyce DW, DiMeglio JL, et al. Directing the outcome of CO_2 reduction at bismuth cathodes using varied ionic liquid promoters. ACS Catal 2018;8:2857–63.
[24] Min X, Kanan MW. Pd-catalyzed electrohydrogenation of carbon dioxide to formate: high mass activity at low overpotential and identification of the deactivation pathway. J Am Chem Soc 2015;137:4701–8.
[25] Gao S, Lin Y, Jiao X, et al. Partially oxidized atomic cobalt layers for carbon dioxide electroreduction to liquid fuel. Nature 2016;529:68.
[26] Han N, Wang Y, Yang H, et al. Ultrathin bismuth nanosheets from *in situ* topotactic transformation for selective electrocatalytic CO_2 reduction to formate. Nat Commun 2018;9:1320.
[27] Koh JH, Won DH, Eom T, et al. Facile CO_2 electro-reduction to formate via oxygen bidentate intermediate stabilized by high-index planes of Bi dendrite catalyst. ACS Catal 2017;7:5071–7.
[28] Zhang W, Hu Y, Ma L, et al. Liquid-phase exfoliated ultrathin Bi nanosheets: uncovering the origins of enhanced electrocatalytic CO_2 reduction on two-dimensional metal nanostructure. Nano Energy 2018;53:808–16.
[29] Chen Z, Mou K, Wang X, et al. Nitrogen-doped graphene quantum dots enhance the activity of Bi_2O_3 nanosheets for electrochemical reduction of CO_2 in a wide negative potential region. Angew Chem Int Ed 2018;130:12972–6.
[30] Deng P, Yang F, Wang Z, et al. Metal-organic frameworks-derived carbon nanorods encapsulated bismuth oxides for rapid and selective CO_2 electroreduction to formate. Angew Chem Int Ed 2020;59:10807–13.
[31] Ma W, Xie S, Zhang XG, et al. Promoting electrocatalytic CO_2 reduction to formate via sulfur-boosting water activation on indium surfaces. Nat Commun 2019;10:892.
[32] Zhang J, Yin R, Shao Q, et al. Oxygen vacancies in amorphous InO_x nanoribbons enhance CO_2 adsorption and activation for CO_2 electroreduction. Angew Chem Int Ed 2019;58:5609–13.
[33] Wen G, Lee DU, Ren B, et al. Orbital interactions in Bi-Sn bimetallic electrocatalysts for highly selective electrochemical CO_2 reduction toward formate production. Adv Energy Mater 2018;8:1802427.
[34] Lei F, Liu W, Sun Y, et al. Metallic tin quantum sheets confined in graphene toward high-efficiency carbon dioxide electroreduction. Nat Commun 2016;7:12697.
[35] Zhang S, Kang P, Meyer TJ. Nanostructured tin catalysts for selective electrochemical reduction of carbon dioxide to formate. J Am Chem Soc 2014;136:1734–7.
[36] Inge AK, Köppen M, Su J, et al. Unprecedented topological complexity in a metal-organic framework constructed from simple building units. J Am Chem Soc 2016;138:1970–6.
[37] Ouyang H, Chen N, Chang G, et al. Selective capture of toxic selenite anions by bismuth-based metal-organic frameworks. Angew Chem Int Ed 2018;57:13197–201.
[38] Liu B, Li C, Zhang G, et al. Oxygen vacancy promoting dimethyl carbonate synthesis from CO_2 and methanol over Zr-doped CeO_2 nanorods. ACS Catal 2018;8:10446–56.
[39] Luo W, Sun L, Yang Y, et al. Cu-Mn composite oxides: highly efficient and reusable acid-base catalysts for the carbonylation reaction of glycerol with urea. Catal Sci Technol 2018;8:6468–77.
[40] Yan A, Liu B, Dong Y, et al. A temperature programmed desorption investigation on the interaction of $Ba_{0.5}Sr_{0.5}Co_{0.8}Fe_{0.2}O_{3-\delta}$ perovskite oxides with CO_2 in the absence and presence of H_2O and O_2. Appl Catal B: Environ 2008;80:24–31.
[41] Zhang Z, Chi M, Veith GM, et al. Rational design of Bi nanoparticles for efficient electrochemical CO_2 reduction: the elucidation of size and surface condition effects. ACS Catal 2016;6:6255–64.
[42] Chu M, Chen C, Guo W, et al. Enhancing electroreduction of CO_2 over Bi_2WO_6 nanosheets by oxygen vacancies. Green Chem 2019;21:2589–93.
[43] Sun X, Zhu Q, Kang X, et al. Molybdenum-bismuth bimetallic chalcogenide nanosheets for highly efficient electrocatalytic reduction of carbon dioxide to methanol. Angew Chem Int Ed 2016;128:6883–7.
[44] Kim S, Wan JD, Gim S, et al. Shape-controlled bismuth nanoflakes as highly selective catalysts for electrochemical carbon dioxide reduction to formate. Nano Energy 2017;39:44–52.
[45] Tang Y-J, Gao M-R, Liu C-H, et al. Porous molybdenum-based hybrid catalysts for highly efficient hydrogen evolution. Angew Chem Int Ed 2015;127:13120–4.
[46] Zhang H, Ma Y, Quan F, et al. Selective electro-reduction of CO_2 to formate on nanostructured Bi from reduction of BiOCl nanosheets. Electrochem Commun 2014;46:63–6.
[47] Lv W, Jing Z, Bei J, et al. Electrodeposition of nano-sized bismuth on copper foil as electrocatalyst for reduction of CO_2 to formate. Appl Surf Sci 2017;393:191–6.
[48] Zhong H, Qiu Y, Zhang T, et al. Bismuth nanodendrites as high performance electrocatalyst for selective conversion of CO_2 to formate. J Mater Chem A 2016;4:13746–53.
[49] Baruch MF, Pander JE, White JL, et al. Mechanistic insights into the reduction of CO_2 on tin electrodes using *in situ* ATR-IR spectroscopy. ACS Catal 2015;5:3148–56.
[50] Chen Y, Kanan MW. Tin oxide dependence of the CO_2 reduction efficiency on tin electrodes and enhanced activity for tin/tin oxide thin-film catalysts. J Am Chem Soc 2012;134:1986–9.

Yi-Rong Wang received her undergraduate degree (2016) and B.S. degree (2019) in Harbin Normal University and Nanjing Normal University, respectively, and now she is a Ph.D. candidate in Nanjing Normal University. Her current research focuses on the synthesis of MOFs-based hybrid electrocatalysts for electrocatalytic reduction of carbon dioxide.

Ru-Xin Yang received her undergraduate degree (2018) in Harbin Normal University, and now she is carrying out her postgraduate life in Nanjing Normal University. At present, she applies herself to make researches on the design and synthesis of highly efficient MOFs-based hybrid electrocatalysts for electrocatalytic reduction of carbon dioxide.

Yifa Chen received his B.S. degree from School of Chemistry, Beijing Institute of Technology. He subsequently obtained his Ph.D. degree from School of Chemistry and Chemical Engineering, Beijing Institute of Technology under the supervision of Prof. Bo Wang. In 2018, he joined Prof. Ya-Qian Lan's group as an associate professor at College of Chemistry and Materials Science of Nanjing Normal University. His research interest focuses on the fabrication of metal–organic framework (MOF) based devices like membranes, foams and fibers that can be applicable in energy storage and conversion, proton conductivity or photo/electric heterogeneous catalysis.

Ya-Qian Lan received his B.S. and Ph.D. degrees (2009) from Northeast Normal University under the supervision of Prof. Zhong-Min Su. In 2010, he joined Prof. Qiang Xu's group at National Institute of Advanced Industrial Science and Technology (AIST, Japan) as a JSPS postdoctoral fellow. Since 2012, he has been a professor of Chemistry at Nanjing Normal University. His current research interests focus on the application of polyoxometalate-based composite materials in energy storage and conversion and porous metal-organic frameworks for applications in catalysis and proton conduction.